

# Lack of large-angle TT correlations persists in *WMAP* and *Planck*

Craig J. Copi,<sup>1</sup>★ Dragan Huterer,<sup>2</sup> Dominik J. Schwarz<sup>3</sup> and Glenn D. Starkman<sup>1,4</sup>

<sup>1</sup>CERCA/Department of Physics/ISO, Case Western Reserve University, Cleveland, OH 44106-7079, USA

<sup>2</sup>Department of Physics, University of Michigan, 450 Church St, Ann Arbor, MI 48109-1040, USA

<sup>3</sup>Fakultät für Physik, Universität Bielefeld, Postfach 100131, D-33501 Bielefeld, Germany

<sup>4</sup>Physics Department, Theory Unit, CERN, CH-1211 Genève 23, Switzerland

Accepted 2015 May 15. Received 2015 April 27; in original form 2014 December 30

## ABSTRACT

The lack of large-angle correlations in the observed microwave background temperature fluctuations persists in the final-year maps from *Wilkinson Microwave Anisotropy Probe (WMAP)* and the first cosmological data release from *Planck*. We find a statistically robust and significant result:  $p$ -values for the missing correlations lying below 0.24 per cent (i.e. evidence at more than  $3\sigma$ ) for foreground cleaned maps, in complete agreement with previous analyses based upon earlier *WMAP* data. A cut-sky analysis of the *Planck HFI* 100 GHz frequency band, the ‘cleanest CMB channel’ of this instrument, returns a  $p$ -value as small as 0.03 per cent, based on the conservative mask defined by *WMAP*. These findings are in stark contrast to expectations from the inflationary Lambda cold dark matter model and still lack a convincing explanation. If this lack of large-angle correlations is a true feature of our Universe, and not just a statistical fluke, then the cosmological dipole must be considerably smaller than that predicted in the best-fitting model.

**Key words:** cosmic background radiation – large-scale structure of Universe.

## 1 INTRODUCTION

The first release of cosmological data from the *Planck* satellite (Planck Collaboration I 2014) and the final analysis of the *Wilkinson Microwave Anisotropy Probe (WMAP)* (Bennett et al. 2013) confirmed that the inflationary Lambda cold dark matter ( $\Lambda$ CDM) model provides an excellent fit to the angular temperature power spectrum for multipoles ranging from the quadrupole ( $\ell = 2$ ) up to  $\ell = 2500$ . The effect of gravitational lensing of the cosmic microwave background (CMB) has been detected with a very high statistical significance ( $25\sigma$ ) (Planck Collaboration XVII 2014) and breaks some parameter degeneracies without reference to non-CMB observations. Most of the statistical power in the *Planck* analysis comes from high- $\ell$  multipoles, thus it may not come as a surprise that the best-fitting model traces the high- $\ell$  data much better than those at low- $\ell$ , where a lack of angular power (in the range  $\ell = 2$  to 32) compared to the best-fitting model is found at the 99 per cent C.L. (Planck Collaboration XV 2014). Nevertheless, it is quite remarkable that none of the models invoking additional, physically well-motivated parameters, such as the sum of neutrino masses, the number of effective relativistic degrees of freedom, or a running of the spectral index, can give rise to a significant improvement of the fit (Planck Collaboration XVI 2014). These findings indicate that some special attention should be devoted to the largest angular

scales, especially as they potentially probe different physics than the small angular scales.

Several anomalies at large angular scales discussed in the literature have been the source of some controversy since the first release of the *WMAP* data (see Bennett et al. 2011; Copi et al. 2010 for reviews). The first of them was already seen by the *Cosmic Background Explorer (COBE)*: the temperature two-point angular correlation function computed as an average over the complete sky

$$C(\theta) = \overline{T(\hat{\mathbf{e}}_1)T(\hat{\mathbf{e}}_2)}, \quad \hat{\mathbf{e}}_1 \cdot \hat{\mathbf{e}}_2 = \cos \theta, \quad (1)$$

was found to be smaller than expected at large angular scales (Hinshaw et al. 1996). Scant attention was given to this observation, due in part to the relatively low signal-to-noise ratio of the *COBE* observations, but mostly to the theory-driven shift in attention away from the angular correlation function and towards the angular power spectrum. The lack of correlations on angular scales larger than  $60^\circ$  was rediscovered almost a decade later by *WMAP* in their one-year analysis (Spergel et al. 2003) and analysed in greater detail by us for the *WMAP* three and five-year data releases (Copi et al. 2009). We have emphasized its persistence in the data (contrary to some claims), differentiated it from the lowness of the temperature quadrupole with which it is often confused, and demonstrated how it challenges the canonical theory’s fundamental prediction of Gaussian random, statistically isotropic temperature fluctuations. For related work on the missing large-angle correlations, see also Copi et al. (2007), Hajian (2007), Sarkar et al. (2011), Kim & Naselsky (2011), Zhang (2012), Gruppuso (2014).

\* E-mail: [cjc5@cwru.edu](mailto:cjc5@cwru.edu)

The *Planck* team presented an analysis of the angular two-point correlation function at a low resolution ( $N_{\text{side}} = 64$ ) for their four component separation methods (Commander–Ruler, NILC, SEVEM, SMICA) after the U73 mask was used to suppress Galactic residuals. Based on comparison with  $10^3$  realizations of the best-fitting model, they find that the probability of obtaining a  $\chi^2$  between the expected angular two-point correlation function of the best-fitting model and the observed correlation function that is at least as large as that measured is 0.883, 0.859, 0.884, and 0.855 for the Commander–Ruler, NILC, SEVEM, and SMICA maps, respectively (Planck Collaboration XXIII 2014). However, their statistic fails to capture that what is anomalous about the angular two-point correlation function is not the extent to which it deviates from the theoretical expected value of the function. Rather, as has been the case since the *COBE-DMR* observation, the pertinent anomaly is that above about  $60^\circ$  the angular correlation function is very nearly zero. It is this very special way of deviating from our expectation that deserves our attention.

In this work, we analyse the two-point angular correlation function at large angles as seen in the final data release of *WMAP* and the first cosmology release of *Planck*. The anomalous alignments of low multipole modes with each other and with directions defined by the geometry and motion of the Solar system are discussed in a companion paper (Copi et al. 2015). Here we demonstrate that on the part of the sky outside the plane of the Galaxy the absence of two-point angular correlations above about  $60^\circ$  remains a robust, statistically significant result, with a  $p$ -value between about 0.03 and 0.33 per cent depending on the precise map and Galaxy cut being analysed.

## 2 PHYSICS AT LARGE ANGULAR SCALES

High fidelity measurements of the microwave sky reveal the imprints of primary temperature, density and metric fluctuations in the early Universe. By observing these fluctuations and analysing their statistical properties, we seek a deeper understanding of cosmological inflation or any alternative mechanism that produced the initial fluctuations.

Studying modes with wavelengths too large to enable causal contact across the mode during the radiation and most of the matter-dominated epochs suggests that we can learn something about the physics of inflation without detailed knowledge of the recent content of the Universe and associated astrophysical details (e.g. reionization). This motivates us to pay special attention to the largest angular scales. Comoving scales that cross into the Hubble radius at  $z \sim 1$  and below are observed at angles larger than  $60^\circ$ . Thus features observed at those scales are either of primordial nature or stem from physics at  $z \lesssim 1$ , the epoch in the history of the Universe that we arguably know best.

To be more precise, at  $z = 0.91(1.5, 7)$  the comoving Hubble length equals the length of a comoving arc with an opening angle of  $90^\circ(60^\circ, 18^\circ)$  for the best-fitting  $\Lambda$ CDM model. These angular scales correspond roughly to the scales that have been shown to be anomalous in previous works (the quadrupole, octopole, and up to modes  $\ell = 10$ ). It is possibly noteworthy that  $z \sim 7$  corresponds to the moment when the Universe is fully reionized.

For better or worse, however, the large-angle CMB is also sensitive to the physics that affects the microwave photons as they propagate from their last scattering until their collection by our telescopes. The late-time integrated Sachs–Wolfe (ISW) effect could potentially correlate the large-angle CMB with the local structure of the gravitational potential. Indeed, it has been proposed in the literature that some of the observed CMB anomalies could be explained

in this way (Rakić, Räsänen & Schwarz 2006; Francis & Peacock 2010; Dupé et al. 2011; Rassat & Starck 2013). Although reconstruction of the local gravitational potential from existing CMB and large-scale structure data is quite uncertain and subject to biases, such an explanation would indeed be an attractive possibility if only there were no lack of correlations on large scales. If the observed lack of large-angle correlations is real, then we must explain how the local gravitational potential manages to align with the primordial temperature fluctuations in such a way that the resulting sky has such a deficit. In the end this does not change the underlying problem; it merely rephrases it from one about the CMB to one about the local gravitational potential.

Clearly, it is important to understand the lack of correlations at large angular scales in greater detail not just for its own sake, but also in order to evaluate any proposed explanation for other features of the CMB data, especially other large-angle or low- $\ell$  anomalies.

## 3 TEMPERATURE TWO-POINT ANGULAR CORRELATION FUNCTION

### 3.1 Theory

In the standard CMB analysis a full-sky map of temperature fluctuations,  $T(\hat{\mathbf{e}})$ , is expanded in spherical harmonics as

$$T(\hat{\mathbf{e}}) = \sum_{\ell m} a_{\ell m} Y_{\ell m}(\hat{\mathbf{e}}), \quad (2)$$

where the coefficients in the expansion are extracted from the full-sky as

$$a_{\ell m} = \int T(\hat{\mathbf{e}}) Y_{\ell m}^*(\hat{\mathbf{e}}) d\hat{\mathbf{e}}. \quad (3)$$

From these quantities we define the angular power spectrum as

$$\mathcal{C}_\ell \equiv \frac{1}{2\ell + 1} \sum_m |a_{\ell m}|^2. \quad (4)$$

Note that the angular power spectrum may *always* be defined in this way. Only in the case of Gaussian random, statistically isotropic temperature fluctuations will contain *all* the statistical information. The full-sky two-point angular correlation function (1) is related to the full-sky angular power spectrum via a Legendre series

$$\mathcal{C}(\theta) = \sum_\ell \frac{2\ell + 1}{4\pi} \mathcal{C}_\ell P_\ell(\cos \theta), \quad (5)$$

where the  $P_\ell(\cos \theta)$  are Legendre polynomials.

Unfortunately the full-sky cannot be observed due to foreground contamination. If we let  $W(\hat{\mathbf{e}})$  represent a mask on the sky (in the simplest case it is zero for pixels removed and one for those included) then cut-sky quantities can be defined in analogy to the full-sky ones from above. In particular, the cut-sky two-point angular correlation function is defined as the sky average,

$$\mathcal{C}^{\text{cut}}(\theta) \equiv \overline{W(\hat{\mathbf{e}}_1) T(\hat{\mathbf{e}}_1) W(\hat{\mathbf{e}}_2) T(\hat{\mathbf{e}}_2)} \\ \equiv \frac{\sum_{ij} W(\hat{\mathbf{e}}_i) T(\hat{\mathbf{e}}_i) W(\hat{\mathbf{e}}_j) T(\hat{\mathbf{e}}_j)}{\sum_{ij} W(\hat{\mathbf{e}}_i) W(\hat{\mathbf{e}}_j)}, \quad \hat{\mathbf{e}}_i \cdot \hat{\mathbf{e}}_j = \cos \theta, \quad (6)$$

where the sums are over all pairs of pixels separated by an angle  $\theta$ . This correlation function can be evaluated in harmonic space by first expanding the cut-sky in pseudo- $a_{\ell m}$  as

$$W(\hat{\mathbf{e}}) T(\hat{\mathbf{e}}) = \sum_{\ell m} \tilde{a}_{\ell m} Y_{\ell m}(\hat{\mathbf{e}}), \quad (7)$$

where

$$\tilde{a}_{\ell m} = \int W(\hat{\mathbf{e}}) T(\hat{\mathbf{e}}) Y_{\ell m}^*(\hat{\mathbf{e}}) d\hat{\mathbf{e}}. \quad (8)$$

From these the pseudo- $\mathcal{C}_\ell$  are defined by

$$\tilde{\mathcal{C}}_\ell \equiv \frac{1}{2\ell + 1} \sum_m |\tilde{a}_{\ell m}|^2. \quad (9)$$

Following Chon et al. (2004) it can be shown that

$$\mathcal{C}^{\text{cut}}(\theta) = 2\pi A(\theta) \sum_\ell (2\ell + 1) \tilde{\mathcal{C}}_\ell P_\ell(\cos \theta). \quad (10)$$

Here the normalization,  $A(\theta)$ , depends on the mask and may be calculated in harmonic space as

$$\frac{1}{A(\theta)} = 2\pi \sum_\ell (2\ell + 1) w_\ell P_\ell(\cos \theta), \quad (11)$$

where

$$w_\ell \equiv \frac{1}{2\ell + 1} \sum_m |w_{\ell m}|^2 \quad (12)$$

and the  $w_{\ell m}$  are coefficients from the spherical harmonic expansion of the mask,

$$W(\hat{\mathbf{e}}) = \sum_{\ell m} w_{\ell m} Y_{\ell m}(\hat{\mathbf{e}}). \quad (13)$$

Notice that for the full-sky  $w_{\ell m} = \sqrt{4\pi} \delta_{\ell 0} \delta_{m0}$  so that  $2\pi A(\theta) = 1/4\pi$  and the cut-sky expansion (10) reproduces the full-sky result (5), as it must. Finally, since  $\mathcal{C}^{\text{cut}}(\theta)$  is a function defined on the interval  $-1 \leq \cos \theta \leq 1$  it may be expanded in a Legendre series as

$$\mathcal{C}^{\text{cut}}(\theta) = \sum_\ell \frac{2\ell + 1}{4\pi} \mathcal{C}_\ell^{\text{cut}} P_\ell(\cos \theta). \quad (14)$$

Note that it is common to just refer to  $\mathcal{C}(\theta)$  as a single quantity covering both the full- and cut-sky cases. It should be remembered that whenever a cut-sky  $\mathcal{C}(\theta)$  is discussed it is defined as in equation (6) and it may be expanded in a Legendre series using the cut-sky  $\mathcal{C}_\ell$  as in equation (14).

For a statistically isotropic universe the ensemble average of the pseudo- $\mathcal{C}_\ell$  (9) is related to the ensemble average of  $\mathcal{C}_\ell^{\text{cut}}$  through a mode coupling matrix (Hauser & Peebles 1973) and  $\mathcal{C}_\ell^{\text{cut}}$  provides an unbiased estimator of the theoretical (full-sky) angular power spectrum (4). Lacking statistical isotropy or some other model the cut-sky angular power spectrum,  $\mathcal{C}_\ell^{\text{cut}}$ , can still be related to the pseudo- $\mathcal{C}_\ell$  through the same mode coupling matrix (see Pontzen & Peiris 2010 for a proof of this result); however the utility of the  $\tilde{\mathcal{C}}_\ell$  or  $\mathcal{C}_\ell^{\text{cut}}$  as estimators of the full-sky or theoretical angular power spectrum would be completely unknown in that case.

It should be emphasized that the mathematical connection between cut-sky quantities,  $\mathcal{C}^{\text{cut}}$  and  $\mathcal{C}_\ell^{\text{cut}}$ , and  $\tilde{\mathcal{C}}_\ell$  does not rely on assumptions from a theory. However, when measured quantities are to be related to the properties of the ensemble predicted by a theory assumptions such as Gaussianity and statistical isotropy become important and must be identified. Thus, to construct an estimator of the theoretical angular power spectrum from cut-sky observations – either through the pseudo- $\mathcal{C}_\ell$  or a maximum-likelihood technique – extra assumptions are required. These assumptions may not be valid on large scales (or low- $\ell$ ) even if they work well on small scales (or high- $\ell$ ).

The simple point being made here is that masking removes information from a map. Without assumptions regarding the properties

of this information it cannot be reinserted when a full-sky map is created. Not even the statistical properties of this information can be known without extra assumptions. In fact, the need for masking of a CMB map is precisely due to contaminations in some regions of the sky. These contaminated regions are excised from the map so as to not affect deduced properties of the underlying theory. Without assumptions a *unique reconstruction of a full-sky map (or any quantity relying on the properties of the masked regions) cannot be computed sensibly*. Particular assumptions may be reasonable or expected to be valid, regardless, such assumptions are required if the full-sky is to be reconstructed and are not required when working solely with cut-sky quantities. For this reason the cut-sky two-point angular correlation function will be the sole focus of this work.

At high- $\ell$ , observed deviations from Gaussianity agree with the amount of non-Gaussianity expected from the non-linear contributions of gravitational lensing (Planck Collaboration XXIV 2014). However, at low- $\ell$ , there are statistically significant anomalies in the temperature map, such as the alignments of multipoles and the hemispherical power asymmetry (Copi et al. 2015; Planck Collaboration XXIII 2014), that are evidence of correlations among the  $a_{\ell m}$  (for different values of  $\ell$  and  $m$ ), and thus contradict the assumption of Gaussian-random statistically isotropic  $a_{\ell m}$ . This suggests that the physics underlying the observed sky cannot be characterized solely by the  $\mathcal{C}_\ell$ , the statistical quantities prescribed by the canonical model; unless these anomalies are unfortunate ‘flukes’, other statistical tools are not just interesting but necessary. The difficulty comes in identifying which are the appropriate ones. The resolution clearly depends on the physics underlying the anomalies. At least until that physics is established, multiple approaches will need to be explored.

### 3.2 Analysis of observations

The two-point temperature angular correlation function for the CMB,  $\mathcal{C}^{TT}(\theta)$ , has remained mostly unchanged since first measured by the COBE-DMR (Hinshaw et al. 1996). The resulting curves from the *Planck* SMICA map are shown in Fig. 1. What is most striking at first glance may be the difference between the best-fitting  $\Lambda$ CDM

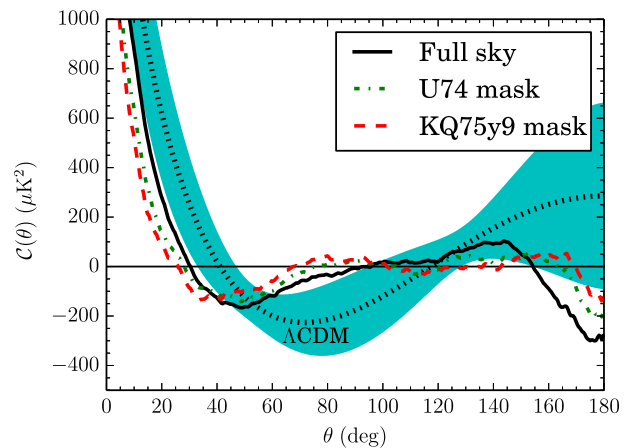


**Figure 1.** Two-point angular correlation function from the inpainted *Planck* SMICA map. The black, dotted line shows the best-fitting  $\Lambda$ CDM model from *Planck*. The shaded, cyan region is the 68 per cent cosmic variance confidence interval. Included from the SMICA map are the  $\mathcal{C}(\theta)$  calculated on the full-sky (black, solid line) and from two cut skies using the U74 mask (green, dash-dotted line) and the KQ75y9 mask (red, dashed line). See the text for details.

model and the observed  $\mathcal{C}(\theta)$  on both the full and cut skies (the details of the masks will be discussed below). This is a source of considerable confusion and great care must be taken to not read too much into this. The values of  $\mathcal{C}(\theta)$  at different angular separations  $\theta$  (or more precisely in different angular bins) are correlated, so the sizeable deviation between the expected  $\Lambda\text{CDM}$  and the observed curves is not as significant as it may appear. Rather, it is the very small value of the observed  $\mathcal{C}(\theta)$  on large angular scales that is truly surprising. This is particularly true for the cut skies where there are essentially no correlations above about  $60^\circ$ , except for some small anti-correlation near  $180^\circ$ .

To quantify this lack of correlations on large angular scales we continue to use the statistic first proposed in the *WMAP* one-year analysis (Spergel et al. 2003),

$$S_{1/2} \equiv \int_{-1}^{1/2} [\mathcal{C}(\theta)]^2 d(\cos \theta) = \sum_{\ell=2}^{\ell_{\max}} \mathcal{C}_\ell I_{\ell\ell'} \mathcal{C}_{\ell'} \quad (15)$$

As discussed above, this definition applies to both full-sky and cut-sky maps. For the case of full-sky maps the full-sky  $\mathcal{C}_\ell$  from equation (4) are used in the sum on the right-hand side, whereas for the case of cut-sky maps the cut-sky  $\mathcal{C}_\ell^{\text{cut}}$  from equation (14) are used. Throughout we will either refer to the  $S_{1/2}$  statistic generically or make it clear the context in which it is calculated. This statistic has not been optimized in any way, except crudely by the choice of the limits of integration, particularly the upper one which has been chosen to be a convenient value. We consistently resist the temptation to optimize these limits in order to minimize the oft-repeated criticism that the statistic is *a posteriori*. In acknowledgement and partial response to that objection, we note that the statistical significance of the absence of large-angle correlations is not particularly dependent either on the precise value of either limit (so long as the range of integration focuses on large scales) or on the particular choice of reasonable integrand.<sup>1</sup>

The sum in equation (15) shows how to quickly and easily calculate  $S_{1/2}$  in terms of the  $\mathcal{C}_\ell$  or  $\mathcal{C}_\ell^{\text{cut}}$  from the Legendre series (5) or (14). The  $I_{\ell\ell'}$  are the components of a matrix of integrals over products of Legendre polynomials and are simply related to the  $\mathcal{I}_{\ell\ell'}(1/2)$  calculated in appendix A of Copi et al. (2009) by  $(4\pi)^2 I_{\ell\ell'} = (2\ell + 1)(2\ell' + 1)\mathcal{I}_{\ell\ell'}(1/2)$ . The sum in the  $S_{1/2}$  expression (15) ranges from  $\ell = 2$  to  $\ell = \ell_{\max}$ . The lower limit is due to the monopole and dipole being removed from the map. We remove the monopole both because its amplitude is significantly larger than those of the other multipoles and because we are interested in the correlations among fluctuations not in the background value. We remove the entire dipole because it is dominated by the Doppler dipole – the (uninteresting) contribution due to our peculiar motion through the Universe; this is approximately two orders of magnitude larger than the expected underlying dipole in the CMB rest frame. Once it is possible to measure the Doppler contribution to better than 1 per cent, it will be far preferable to remove the Doppler dipole, and set  $\ell = 1$  as the lower limit of the sum in expression (15). For the upper limit there is some freedom in the choice of  $\ell_{\max}$ .

<sup>1</sup> In another paper, looking at the predictions for the two-point angular correlation function of temperature with polarization, specifically the  $Q$  Stokes parameter (Copi et al. 2013), we optimized the upper and lower limits of integration, and considered both  $[\mathcal{C}^{TQ}(\theta)]^2$  and  $\mathcal{C}^{TQ}(\theta)$  as integrands in the equivalent of (15). However, in that case we were *a priori* optimizing a statistic for a specific purpose – differentiating between two models. Furthermore, it was found that replacing  $[\mathcal{C}^{TQ}(\theta)]^2$  in the integrand with  $\mathcal{C}^{TQ}(\theta)$  makes no qualitative difference in the conclusions.

**Table 1.** Smallness of  $S_{1/2}$  for maps without the DQ correction. We analyse the cleaned maps from *Planck*: NILC, SEVEM, and SMICA, as well as from *WMAP*: seven- and nine-year ILC. We also analyse the individual frequency band maps from *Planck*: HFI 100 GHz and LFI 70 GHz, as well as from *WMAP*: seven- and nine-year *W* and *V* bands. For each map, we use both the U74 and KQ75y9 masks. In all cases residual monopole and dipole contributions have been subtracted from the map after masking. For each map and mask we report the  $S_{1/2}$  value and the associated  $p$ -value – the fraction of realizations of  $\Lambda\text{CDM}$  in the *Planck* best-fitting  $\Lambda\text{CDM}$  model with an  $S_{1/2}$  no larger than the reported value.

| Map                        | U74                                      |                | KQ75y9                                   |                |
|----------------------------|--|----------------|--|----------------|
|                            | $S_{1/2}$ ( $\mu\text{K}$ ) <sup>4</sup> | $p$ (per cent) | $S_{1/2}$ ( $\mu\text{K}$ ) <sup>4</sup> | $p$ (per cent) |
| WMAP ILC 7yr               | 1582.3                                   | 0.193          | 1225.8                                   | 0.085          |
| WMAP ILC 9yr               | 1626.0                                   | 0.211          | 1278.2                                   | 0.100          |
| Planck SMICA               | 1577.7                                   | 0.191          | 1022.3                                   | 0.044          |
| Planck NILC                | 1589.3                                   | 0.195          | 1038.2                                   | 0.047          |
| Planck SEVEM               | 1657.7                                   | 0.225          | 1153.4                                   | 0.069          |
| WMAP W 7yr                 | 1863.6                                   | 0.316          | 1133.9                                   | 0.065          |
| WMAP W 9yr                 | 1887.1                                   | 0.329          | 1142.6                                   | 0.068          |
| Planck HFI 100             | 1682.1                                   | 0.235          | 911.6                                    | 0.027          |
| WMAP V 7yr                 | 1845.0                                   | 0.307          | 1290.9                                   | 0.104          |
| WMAP V 9yr                 | 1850.0                                   | 0.309          | 1281.8                                   | 0.101          |
| Planck LFI 70 <sup>a</sup> | —  | —              | —  | —              |

Notes. <sup>a</sup>The calibration of the *Planck* LFI 70 GHz channel includes the DQ correction. See Planck Collaboration V (2014) and Copi et al. (2015) for details.

**Table 2.** Same as Table 1 now with the DQ-corrected maps.

| Map            | U74                                      |                | KQ75y9                                   |                |
|----------------|--|----------------|--|----------------|
|                | $S_{1/2}$ ( $\mu\text{K}$ ) <sup>4</sup> | $p$ (per cent) | $S_{1/2}$ ( $\mu\text{K}$ ) <sup>4</sup> | $p$ (per cent) |
| WMAP ILC 7yr   | 1620.3                                   | 0.208          | 1247.0                                   | 0.090          |
| WMAP ILC 9yr   | 1677.5                                   | 0.232          | 1311.8                                   | 0.109          |
| Planck SMICA   | 1606.3                                   | 0.202          | 1075.5                                   | 0.053          |
| Planck NILC    | 1618.6                                   | 0.208          | 1096.2                                   | 0.058          |
| Planck SEVEM   | 1692.4                                   | 0.239          | 1210.5                                   | 0.082          |
| WMAP W 7yr     | 1839.0                                   | 0.304          | 1128.5                                   | 0.064          |
| WMAP W 9yr     | 1864.2                                   | 0.317          | 1138.3                                   | 0.066          |
| Planck HFI 100 | 1707.5                                   | 0.245          | 916.3                                    | 0.028          |
| WMAP V 7yr     | 1829.2                                   | 0.300          | 1276.2                                   | 0.099          |
| WMAP V 9yr     | 1840.4                                   | 0.304          | 1268.8                                   | 0.097          |
| Planck LFI 70  | 1801.7                                   | 0.287          | 1282.1                                   | 0.101          |

Since  $\mathcal{C}_\ell \sim \ell^{-2}$  we would expect that the result is independent of our choice provided that  $\ell_{\max}$  is ‘large enough’. However, since we will find small values of  $S_{1/2}$ , the exact choice does have a slight effect on the final values. We have consistently chosen  $\ell_{\max} = 100$  for all calculations of  $S_{1/2}$  in this work. The effect of this choice on the value of  $S_{1/2}$  depends on the map and mask employed but is always less than one per cent (for  $\ell_{\max} \geq 100$ ). For example, using a larger value of  $\ell_{\max}$  with the *Planck* SMICA full-sky map the maximum deviation in  $S_{1/2}$  is about 0.08 per cent. For this map and the U74 mask the maximum deviation is about 0.4 per cent. Larger variations in the  $S_{1/2}$  value occur between the maps as seen in Tables 1 and 2. For example, in Table 1 there is a 0.7 per cent change between the  $S_{1/2}$  value for the *Planck* SMICA and NILC maps with the U74 mask; however, even this difference only corresponds to a change in the third digit in the  $p$ -value (from 0.191 to 0.195). In practice, the choice of  $\ell_{\max}$  should be used consistently in analysing both the data and realizations which will further mitigate its effect.

The calculation of  $S_{1/2}$  has therefore been reduced to finding the angular power spectrum either over the full-sky or cut-sky for some map of the CMB temperature. However, a number of important choices must be made, which we now discuss.

First, there are a number of maps available for analysis. In each data release, the *WMAP* team included individual band maps and a full-sky Independent Linear Combination (ILC) map designed to be as close to the foreground-subtracted CMB as possible. The *Planck* team released individual band maps and three different foreground-subtracted maps – NILC, SEVEM, SMICA – in their initial 2013 release, although they had many more, including one they called the Commander–Ruler map.<sup>2</sup> Here we will analyse the seven and nine-year *WMAP* *V* and *W* band maps and the ILC map, the *Planck* High Frequency Instrument (*HFI*) 100 GHz and Low Frequency Instrument (*LFI*) 70 GHz maps (these two channels are expected to be least contaminated by foregrounds), and its NILC, SEVEM, and SMICA maps.<sup>3</sup>

Once we have a map, we must also choose the resolution of the maps to be analysed. A higher resolution will minimize resolution-dependent effects. On the other hand, to reduce the computation time, particularly when generating statistics from realizations of  $\Lambda\text{CDM}$ , a low resolution is preferred. As a compromise we have chosen the HEALPix<sup>4</sup> resolution  $N_{\text{side}} = 128$  for all studies in this work.

To work at  $N_{\text{side}} = 128$  we degrade the high-resolution maps by averaging over pixels using `ud_grade` from HEALPix. This process follows that used for degrading the masks discussed below. To gain a computational advantage from working at lower resolution, realizations are generated at  $N_{\text{side}} = 128$  directly. Further, they are only generated including modes up to  $\ell_{\max} = 100$ . It has been verified that neither degrading from higher resolutions realizations nor increasing  $\ell_{\max}$  affects the final results. This is not surprising given that  $S_{1/2}$  is only weakly dependent on small scale and large- $\ell$  behaviour.

Even with the existence of cleaned, full-sky maps the concern of residual contamination, particularly on the largest angular scales, remains. For this reason it is desirable to remove the most contaminated regions of the sky and only analyse the cleanest ones. The *Planck* analysis used the U73 mask which leaves a sky fraction  $f_{\text{sky}} = 0.73$  (Planck Collaboration XXIII 2014). This mask is not publicly available but is constructed from the union of the validity masks provided with the full-sky maps (Planck Collaboration XII 2014). For the NILC, SEVEM, and SMICA maps these masks are available. For the Commander–Ruler map only a minimal version of the mask is provided. Taking the union of these four masks produces what we call the U74 mask, a close approximation of the U73 mask but with  $f_{\text{sky}} = 0.74$ . For *WMAP* we use their extended temperature mask from their nine-year data release, named KQ75y9, which has  $f_{\text{sky}} = 0.69$ .

These masks are provided at high resolution;  $N_{\text{side}} = 2048$  for the U74 mask and  $N_{\text{side}} = 1024$  for the KQ75y9 mask. To degrade the masks to our working resolution of  $N_{\text{side}} = 128$  we follow the prescription defined in Planck Collaboration XXIII (2014): first the

<sup>2</sup> The Commander–Ruler map was subsequently released after this study was completed.

<sup>3</sup> All CMB data are available from the Lambda site, <http://lambda.gsfc.nasa.gov/>, including links to both *WMAP* and *Planck* results. The *Planck* results may directly be obtained via the *Planck* Legacy Archive, <http://archives.esac.esa.int/pla/>.

<sup>4</sup> The HEALPix source code is freely available from healpix.sourceforge.net.

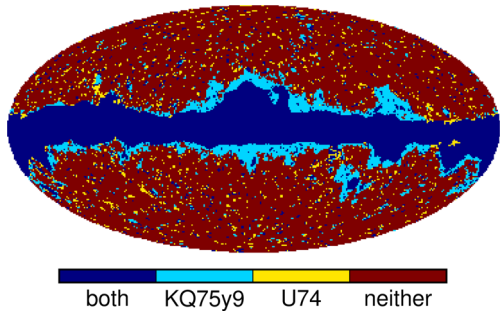


**Figure 2.** Masks used in this work. A pixel may be removed by both masks (dark blue), only the KQ75y9 mask (light blue), only the U74 mask (yellow), or by neither mask (red).

mask is degraded to  $N_{\text{side}} = 128$  using `ud_grade` from HEALPix, then any pixel with a value less than 0.8 is set to zero, otherwise it is set to one. With this prescription the  $N_{\text{side}} = 128$  masks have sky fractions of  $f_{\text{sky}} = 0.72$  for U74 and  $f_{\text{sky}} = 0.67$  for KQ75y9.

Despite the KQ75y9 mask removing more pixels, the U74 mask is not fully contained within it. A comparison of the two masks is given in Fig. 2. As can be seen, the two masks mostly coincide, though there are many small regions of pixels only contained in one of the two masks. In particular, there are pixels that are excluded by the U74 mask but included by the KQ75y9 mask and the KQ75y9 mask generally removes more of the region around the Galactic Centre than the U74 mask. These small differences have a noticeable effect on the calculated cut-sky  $S_{1/2}$ .

It is important that comparisons of data and simulations are made consistently. In addition to the choices discussed above, cut-sky data will always be compared to cut-sky realizations, with the maps in all cases treated as similarly as possible. This is particularly important since, as noted above, for cut skies the cut-sky  $C_\ell$  are employed in the calculation of  $S_{1/2}$ . In this work we are *not* interested in reconstructing the full-sky angular correlations. Instead, we find that angular correlations on the cut-sky are unusually low. We thus do not make statements about the full-sky CMB, which at any rate cannot be reliably observed, and for which a maximum-likelihood estimator may be more appropriate (Efstathiou 2004; Efstathiou, Ma & Hanson 2010; Pontzen & Peiris 2010). Even so, reconstructing the full-sky from a cut-sky requires extra assumptions and may introduce its own biases (Copi et al. 2011).

Extracting the  $C_\ell$  from a map, particularly from a masked map, also requires some care. We use SPICE (Chon et al. 2004) for this purpose since it calculates the  $C_\ell^{\text{cut}}$  which appear in the Legendre series (14). For cut skies there is the added issue that even if the full-sky does not include a monopole or dipole, these modes will exist in the portion of the sky included for evaluation. If we knew that the full-sky map did not contain a residual monopole or dipole, then we could proceed without further concern. Unfortunately, with real data this is not known, particularly for individual frequency band maps which definitely have Galactic contamination. We therefore remove the average monopole and dipole from all maps prior to extracting the  $C_\ell$ . For the monopole, we do this by subtracting the average value of the temperature over the portion of the sky that is being retained; for the dipole we find the best-fitting dipole over the retained sky and subtract that dipole. (In SPICE this removal is a built-in feature which we employ in our analysis.) When analysing a cut-sky, this procedure generically introduces a monopole and dipole (and alters the other multipoles) into the equivalent full-sky map. Though this may seem to be a problem, again recall that the

cut-sky analysis is self-contained and internally consistent since the data and realizations are treated identically. The cut-sky statistics are *not* estimators of the full-sky, as again made clear by this monopole and dipole removal.

There is also the question of the effect of our motion with respect to the CMB rest frame on the quadrupole. Just as that motion, with velocity  $\beta \equiv v/c \sim 10^{-3}$ , induces a dipole with amplitude  $\mathcal{O}(\beta)$  times the monopole, it also induces a Doppler quadrupole (DQ) with amplitude  $\mathcal{O}(\beta^2)$  times the monopole. The naive expectation that since  $\beta^2 \sim 10^{-6}$  the DQ will be an unimportant contribution to the cosmological quadrupole is not obviously true at least in part because the measured quadrupole is much smaller than the theoretical expectation. For each map we analyse both the DQ uncorrected and the DQ corrected map to gauge the importance of this effect. The one exception is the *Planck LFI* 70 GHz map, where (at least part of) the DQ has been accounted for in the calibration procedure. See Planck Collaboration V (2014), Copi et al. (2015) for a more detailed discussion on this issue.

The effect of the boosted blackbody DQ correction on  $S_{1/2}$  is shown in Tables 1 and 2 where it is found that the effect on  $p$ -values is much less than the differences among the *Planck* maps, and is thus not significant. The DQ correction is frequency-dependent, and subsequent to this analysis Planck Collaboration XXIII (2014) was updated to include estimates of DQ correction factors for each of their released combined maps. Since neither a complete description of how these correction factors were calculated nor all the data required to calculate such correction factors were made publicly available, and since the effect on  $S_{1/2}$  was negligible from the simple estimate of the DQ correction, these correction factors have not been included in our analysis.

#### 4 RESULTS

Histograms of  $S_{1/2}$  values from  $10^6$  realizations of the *Planck* best-fitting  $\Lambda$ CDM model (based on their temperature only data) are shown in Fig. 3. Included in the figure are the full-sky and cut-sky  $S_{1/2}$ . As seen in the figure, masking has a small effect; the peak of the distribution is shifted to slightly smaller values due to masking, but this does not have a noticeable change on the tail of the distribution.

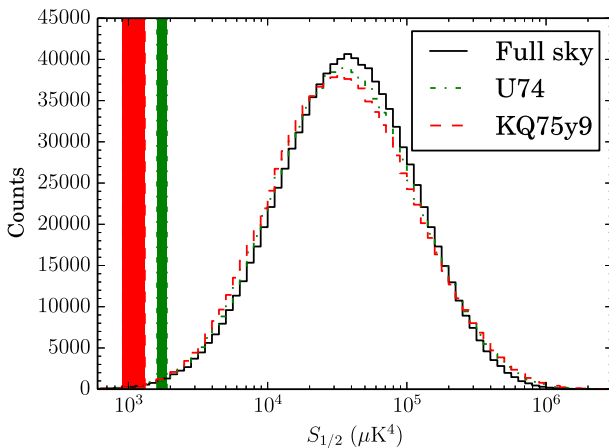


**Figure 3.** Distribution of  $S_{1/2}$  values from  $10^6$  realizations of the best-fitting  $\Lambda$ CDM model for full and masked skies. The shaded regions (green, dash-dotted for the U74 mask and red, dashed for the KQ75y9 mask) represent the spread of the observed values as given in Tables 1 and 2. Masking only slightly affects the expected distributions and the observations are in the small  $S_{1/2}$  tail of the distribution for both masks considered in this work.

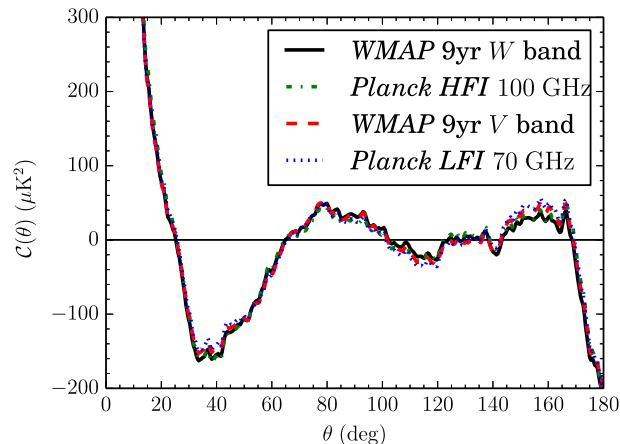


**Figure 4.** Cut-sky  $C(\theta)$  using the KQ75y9 mask for individual frequency band maps. Shown are correlation functions from the *WMAP* nine-year *W* (black, solid line) and *V* (red, dashed line) bands along with the *Planck HFI* 100 GHz (green, dash-dotted line) and *LFI* 70 GHz (blue, dotted line) maps. The curves for the *WMAP* seven-year band maps are nearly identical to those from the nine-year maps and are not included for clarity. In all cases the correlation functions are in excellent agreement across the data releases and frequency bands. (Note the range on y-axis has been greatly reduced as compared to Fig. 1 to allow for any difference to be noticeable by eye.)

Regardless, in comparing cut-sky  $S_{1/2}$  between the data and our realizations, we always compare the one set of cut-sky data to the same set of cut-sky realizations.

The  $S_{1/2}$  values for the various map and mask combinations are given in Table 1 for the case when the maps are not DQ corrected and in Table 2 when the DQ correction has been applied. As discussed above, the realization maps are treated precisely like the data maps – they are masked, then monopole and dipole are subtracted before  $S_{1/2}$  is computed. Given that the value of  $S_{1/2}$  on masked skies is extremely low compared to the typical value, having  $10^6$  is necessary to make quantitatively precise statements. For each computed value of  $S_{1/2}$  reported, we also report the  $p$ -value – the fraction of realizations (expressed in per cent) that have an  $S_{1/2}$  at least as low. This we interpret as the probability of obtaining a value of  $S_{1/2}$  this low by random chance in the best-fitting model of  $\Lambda$ CDM.

An alternative approach is to allow for variations of the best-fitting parameters within their error bars, for example by examining a Monte Carlo Markov chain of the parameters rather than just performing realizations of the best-fitting values. [Such an approach was taken for example in Copi et al. (2009).] This will affect the results only weakly, because varying the parameters within their error bars will cause the expected low- $\ell$   $C_\ell$  to vary by much less than their cosmic variance.

The cut-sky  $S_{1/2}$  values presented in Tables 1 and 2 show that the region outside the masks is consistently observed and cleaned in all the data releases mostly independent of analysis procedures. In Fig. 4 we plot  $C(\theta)$  for the *WMAP* nine-year *V* and *W* bands with the KQ75y9 mask and the *Planck HFI* 100 GHz and *LFI* 70 GHz bands also with the KQ75y9 mask. One can see that the cut-sky angular correlation functions are remarkably consistent across instruments and wavebands. (And also across *WMAP* data releases. We have chosen not to plot the *WMAP* seven-year correlation functions because they are nearly indistinguishable from the nine-year functions.) We can thus place great confidence in the cut-sky  $S_{1/2}$  results derived from *WMAP* and *Planck*. These results can be summarized as follows.

(i) Regardless of the maps, the cut-sky  $S_{1/2}$  is very low, with  $p$ -values ranging from 0.027 per cent for the *Planck HFI* 100 GHz map with the KQ75y9 mask to 0.329 per cent for the *WMAP* nine-year W band map with the U74 mask.

(ii) The cleaned maps have a smaller variation in  $S_{1/2}$  values with a  $p$ -value always less than about 0.239 per cent for the U74 mask and less than about 0.109 per cent for the KQ75y9 mask.

(iii) The *Planck* maps typically have smaller  $S_{1/2}$  values than the *WMAP* maps. (The two slight exceptions are the DQ corrected *Planck LFI* 70 GHz band with the KQ75y9 mask and the *Planck SEVEM* map for the U74 mask.)

(iv) The only clear systematic trend is that the KQ75y9 mask consistently yields a lower cut-sky  $S_{1/2}$  than does the U74 mask. Presumably this is due to the larger region around the Galactic Centre excluded by the KQ75y9 mask (see Fig 2).

(v) The DQ correction has little effect, in most cases tending to slightly increase  $S_{1/2}$  in the *Planck* maps and decrease it in the *WMAP* ones. This is in contrast to the importance of applying the DQ correction for full-sky alignment studies (Copi et al. 2015).

Overall, the data very consistently show a lack of correlations on large angular scales outside the Galactic region (as defined by the two masks employed). The  $p$ -value for the  $S_{1/2}$  statistic has remained small and of comparable size throughout the *WMAP* data releases and now with the first *Planck* results. This is remarkable given the improvements in statistics, cleaning, beams, masks, and other systematics. Further, this is in contrast to the full-sky  $S_{1/2}$  which vary significantly from data release to data release and from map to map. The behaviour of the full-sky  $S_{1/2}$  is discussed in more detail in Copi et al. (2015). It suffices here to note that the full-sky value of  $S_{1/2}$  varies from a low of 3766 ( $\mu\text{K}^4$ ), from the *Planck SEVEM* map, to a high of 8938 ( $\mu\text{K}^4$ ), calculated from the seven-year *WMAP* reported values of the angular power spectrum based on a maximum likelihood estimator.

We again emphasize that the two-point angular correlation function that we have calculated is monopole and dipole-subtracted. However, once the Doppler dipole is sufficiently well determined, only it should be removed and the underlying cosmological contribution to the dipole retained in  $\mathcal{C}(\theta)$  and thus in  $S_{1/2}$ .

The measured lack of angular correlations in the dipole-subtracted sky has an important consequence for the primordial dipole. If the missing correlations are not a very unlikely fluke, nor (as our results indicate) due to systematic errors or map-cleaning procedures, then they are caused by some as-yet unidentified physical mechanism. It is difficult to see how such a mechanism would set  $\mathcal{C}(\theta)$  to be nearly zero on angular scales greater than  $60^\circ$  when the primordial dipole is subtracted, and yet somehow not also do so if the dipole were included. Instead, for a physical mechanism we would expect the total angular correlation function including the contribution of the cosmological dipole to also be nearly zero on these scales. In the best-fitting  $\Lambda\text{CDM}$  model, the expected contribution from the dipole alone is very large and generically spoils the vanishing of  $\mathcal{C}(\theta)$  on large angular scales. Hence, if the vanishing correlations are of cosmological origin, then the primordial dipole is also expected to be very suppressed.

To be concrete, the expected value of  $\mathcal{C}_1$  in the best-fitting  $\Lambda\text{CDM}$  model is approximately  $3300 \mu\text{K}^2$ . With this value, the  $\mathcal{C}_1^2$  contribution to  $S_{1/2}$  in equation (15) alone would contribute approximately  $2.3 \times 10^5 \mu\text{K}^4$  to  $S_{1/2}$ . (In principle this could be compensated by the cross term,  $\mathcal{C}_1\mathcal{C}_\ell$  with  $\ell \neq 1$ , which can be negative; however, in practice this does not occur owing mainly to the smallness of  $\mathcal{C}_2$ .) Roughly, for the  $\mathcal{C}_1^2$  contribution to not make the  $S_{1/2}$  ‘too large’

the value of  $\mathcal{C}_1$  must also not be ‘too large’. For example, requiring the contribution to  $S_{1/2}$  to be comparable to current cut-sky values, that is a contribution of the order of  $1000 \mu\text{K}^4$ , places a limit  $\mathcal{C}_1 \lesssim 200 \mu\text{K}^2$ . This has a probability of occurring by chance in a realization of the best-fitting model (due to cosmic variance) of less than approximately 0.4 per cent. Equivalently, to the extent that  $\mathcal{C}_1$  contributions dominate the value of  $S_{1/2}$ , in order to maintain a  $p$ -value for the  $S_{1/2}$  less than 0.4 per cent once the cosmological dipole is included requires that  $\mathcal{C}_1 \lesssim 200 \mu\text{K}^2$ .

To summarize, it seems unlikely that a physical mechanism would predict that the  $S_{1/2}$  calculated from a dipole-subtracted cut-sky would be small but the  $S_{1/2}$  calculated from a non-dipole-subtracted cut-sky would not be. This strongly suggests that if the lack of angular correlations is physical in nature and not a statistical fluke, then a robust prediction can be made that there is a very small cosmological dipole. In a future work we will develop this prediction more precisely.

## 5 CONCLUSIONS

The CMB shows a lack of correlations on large angular scales. This can be quantified by the  $S_{1/2}$  statistics proposed by Spergel et al. (2003) which is best calculated on the portion of the sky outside the Galaxy. Unlike attempts to infer properties of the full-sky correlation function, the cut-sky  $S_{1/2}$  appears remarkably robust and trustworthy. In our analysis we find that the  $p$ -value for the observed cut-sky  $S_{1/2}$  in an ensemble of realizations of the best-fitting  $\Lambda\text{CDM}$  model never exceeds 0.33 per cent for any of the analysed combinations of maps and masks, with and without correcting for the DQ. This has remained the case since the *WMAP* three-year data release,<sup>5</sup> for both the individual (*V* and *W*) band maps and the synthesized (ILC) map, and for the first *Planck* data release for both the *LFI* and *HFI* band maps and all the released synthesized maps (NILC, SMICA, SEVEM), when masked by either the *WMAP* KQ75y9 mask or the less conservative U74 mask (which is very similar to the *Planck* U73 mask). The *HFI* 100 GHz map – the presumably cleanest CMB band of *HFI* – with the more conservative mask that has been defined by *WMAP* gives a  $p$ -value of only 0.03 per cent! As general trends we note that a larger mask tends to produce smaller  $p$ -values; the DQ correction does not change the results in a significant way; and the *Planck* data yield somewhat smaller  $p$ -values than the *WMAP* data.

This apparent lack of temperature correlations on large angular scales is striking. It is a robust observation that increases in statistical significance from *COBE* to *WMAP* to *Planck*. The consistency of the lack of angular correlations greatly reduces the likelihood of instrumental issues as a cause. Since all three missions observed the same sky, we could be unlucky and live in a very atypical realization of the Universe. A method of testing this hypothesis has been proposed that would utilize the upcoming *Planck* polarization data (Copi et al. 2013). If it is not a statistical fluke and not an instrumental issue, it still could be caused by foregrounds. This appears also unlikely as the lack of correlations is consistently seen in individual bands as well as in foreground cleaned maps. Thus, to the best of our knowledge, the lack of angular correlations is in contradiction with the idea of scale invariant, isotropic and Gaussian perturbations seeded by cosmological inflation.

<sup>5</sup> The one-year *WMAP* release yielded slightly higher  $p$ -values – 0.38 per cent for the *V* band, and 0.64 per cent for the *W* band (Copi et al. 2007; Copi et al. 2009).

Attempts to explain this lack of correlations should also address the various other anomalous aspects observed in the microwave sky. It turns out that the lack of angular correlations puts very severe constraints on such models. For example, a plausible explanation for the alignments of multipole vectors or for the hemispherical asymmetry observed might have been contamination by unaccounted foregrounds; however, one cannot easily understand how a hypothetical foreground, which presumably should be uncorrelated with the primordial temperature fluctuations, could cause an almost exact cancellation of the primordial fluctuations at angular scales above  $60^\circ$ .

Several attempts have been made to explain the absence of large-angle correlations as being due to an unknown foreground or, more generally, by altering the procedure by which one arrives at the cleaned maps. Indeed, when the cleaned maps are altered in any way the microwave sky can easily be made to appear less anomalous. This is not surprising; almost any random modification of the observed maps will make them less anomalous. Though the removal of anomalies may be a side effect of improved analysis procedures, using their removal as a basis for judging the effectiveness of such a procedure is misguided.

Finally, we emphasize that in order to be convincing, new theoretical models to explain the observed large-angle anomalies must be based on the statistics of realizations of that model, not just on having the mean values of the model agree with observations. In other words, CMB map realizations based on the underlying new model should have  $p$ -values for the measured statistics that are not unusually small.

The large-angle temperature–temperature correlations in the CMB outside the Galaxy have been anomalously low in all relevant maps since the days of the *COBE-DMR*. The final *WMAP* release and the initial *Planck* release confirm that anomaly. After 20 years, we still await a satisfactory explanation.

## ACKNOWLEDGEMENTS

We acknowledge valuable communications and discussions with F. Bouchet, C. Burigana, J. Dunkley, G. Efstathiou, K. Ganga, P. Naselsky, H. Peiris, C. Räth and D. Scott. GDS and CJC are supported by a grant from the US Department of Energy to the Particle Astrophysics Theory Group at CWRU. DH has been supported by the DOE, NSF, and the Michigan Center for Theoretical Physics. DJS is supported by the DFG grant RTG 1620 ‘Models of gravity’. DH thanks the Kavli Institute for Theoretical Physics and GDS thanks the Theory Unit at CERN for their respective hospitality. This work made extensive use of the HEALPix package (Górski et al. 2005). The numerical simulations were performed on the facilities provided by the Case ITS High Performance Computing Cluster. We acknowledge the use of the Legacy Archive for Microwave Background Data Analysis (LAMBDA), part of the High Energy Astrophysics Science Archive Center

(HEASARC). HEASARC/LAMBDA is a service of the Astrophysics Science Division at the NASA Goddard Space Flight Center. This paper made use of observations obtained with *Planck* (<http://www.esa.int/Planck>), an ESA science mission with instruments and contributions directly funded by ESA Member States, NASA, and Canada.

## REFERENCES

- Bennett C. L. et al., 2011, ApJS, 192, 17  
 Bennett C. L. et al., 2013, ApJS, 208, 20  
 Chon G., Challinor A., Prunet S., Hivon E., Szapudi I., 2004, MNRAS, 350, 914  
 Copi C. J., Huterer D., Schwarz D. J., Starkman G. D., 2007, Phys. Rev. D, 75, 023507  
 Copi C. J., Huterer D., Schwarz D. J., Starkman G. D., 2009, MNRAS, 399, 295  
 Copi C. J., Huterer D., Schwarz D. J., Starkman G. D., 2010, Adv. Astron., 2010, 78  
 Copi C. J., Huterer D., Schwarz D. J., Starkman G. D., 2011, MNRAS, 418, 505  
 Copi C. J., Huterer D., Schwarz D. J., Starkman G. D., 2013, MNRAS, 434, 3590  
 Copi C. J., Huterer D., Schwarz D. J., Starkman G. D., 2015, MNRAS, 449, 3458  
 Dupé F. X., Rassat A., Starck J. L., Fadili M. J., 2011, A&A, 534, A51  
 Efstathiou G., 2004, MNRAS, 348, 885  
 Efstathiou G., Ma Y., Hanson D., 2010, MNRAS, 407, 2530  
 Francis C. L., Peacock J. A., 2010, MNRAS, 406, 14  
 Górski K. M., Hivon E., Banday A. J., Wandelt B. D., Hansen F. K., Reinecke M., Bartelmann M., 2005, ApJ, 622, 759  
 Gruppuso A., 2014, MNRAS, 437, 2076  
 Hajian A., 2007, preprint ([astro-ph/0702723](http://arxiv.org/abs/astro-ph/0702723))  
 Hauser M. G., Peebles P. J. E., 1973, ApJ, 185, 757  
 Hinshaw G., Brandby A. J., Bennett C. L., Górski K. M., Kogut A., Lineweaver C. H., Smoot G. F., Wright E. L., 1996, ApJ, 464, L25  
 Kim J., Naselsky P., 2011, ApJ, 739, 79  
 Planck Collaboration I, 2014, A&A, 571, A1  
 Planck Collaboration V, 2014, A&A, 571, A5  
 Planck Collaboration XII, 2014, A&A, 571, A12  
 Planck Collaboration XV, 2014, A&A, 571, A15  
 Planck Collaboration XVI, 2014, A&A, 571, A16  
 Planck Collaboration XVII, 2014, A&A, 571, A17  
 Planck Collaboration XXIII, 2014, A&A, 571, A23  
 Planck Collaboration XXIV, 2014, A&A, 571, A24  
 Pontzen A., Peiris H. V., 2010, Phys. Rev. D, 81, 103008  
 Rakić A., Räsänen S., Schwarz D. J., 2006, MNRAS, 369, L27  
 Rassat A., Starck J. L., 2013, A&A, 557, L1  
 Sarkar D., Huterer D., Copi C. J., Starkman G. D., Schwarz D. J., 2011, Astropart. Phys., 34, 591  
 Spergel D. N. et al., 2003, ApJS, 148, 175  
 Zhang S., 2012, ApJ, 748, L20

This paper has been typeset from a  $\text{\TeX}$ / $\text{\LaTeX}$  file prepared by the author.